

UNCLASSIFIED

SECURITY CLASSIFICATION OF THIS PAGE

DTIC FILE COPY



REPORT DOCUMENTATION PAGE

Form Approved OMB No. 0704-0188 Exp Date Jun 30, 1986

1a REPORT SECURITY CLASSIFICATION UNCLASSIFIED

1b RESTRICTIVE MARKINGS

2 SECURITY CLASSIFICATION AUTHORITY

3 DISTRIBUTION/AVAILABILITY OF REPORT Published in the open literature

AD-A196 707

5 MONITORING ORGANIZATION REPORT NUMBER(S)

6a NAME OF PERFORMING ORGANIZATION Research Directorate, RD&EC US Army Missile Command

6b OFFICE SYMBOL (if applicable) AMSMI-RD-RE-OP

7a NAME OF MONITORING ORGANIZATION Same as 6a

6c ADDRESS (City, State, and ZIP Code) Redstone Arsenal, AL 35898-5248

7b ADDRESS (City, State, and ZIP Code) Same as 6c

DTIC ELECTED JUN 21 1988

8a NAME OF FUNDING/SPONSORING ORGANIZATION Same as 6a

8b OFFICE SYMBOL (if applicable)

9 PROCUREMENT INSTRUMENT IDENTIFICATION NUMBER

8c ADDRESS (City, State, and ZIP Code) Same as 6c

10 SOURCE OF FUNDING NUMBERS PROGRAM ELEMENT NO PROJECT NO TASK NO WORK UNIT ACCESSION NO

11 TITLE (Include Security Classification) LONGITUDINAL SPATIAL INHOMOGENEITIES IN INTRINSIC OPTICAL BISTABILITY DUE TO INDUCED ABSORPTION (U)

12 PERSONAL AUTHOR(S) Bowden, Charles M., Sung, C. C., Haus, J. W., and Cook, J. M.

13a TYPE OF REPORT Open-Literature

13b TIME COVERED FROM TO

14 DATE OF REPORT (Year, Month, Day) 1988 January

15 PAGE COUNT 9

16 SUPPLEMENTARY NOTATION The report appeared as an open-literature publication in the Journal of the Optical Society of America B, Vol. 5, pages 11-19 (1988).

Table with 3 columns: FIELD, GROUP, SUB-GROUP. Includes COSATI CODES.

18 SUBJECT TERMS (Continue on reverse if necessary and identify by block number) GaAs/GaAlAs; CdS single crystals; quantum-well material; Intrinsic Optical Bistability; Absorption profile, Gallium Arsenide, reprints. (21911)

19 ABSTRACT (Continue on reverse if necessary and identify by block number) Longitudinal spatial effects in the nonlinear medium are analyzed in a model for mirrorless optical bistability due to induced absorption that treats heat conduction, electromagnetic field propagation, and temperature-dependent absorption. We consider two specific cases: the temperature-induced shift of the absorption peak of bound I2 excitons in CdS single crystals and the temperature-induced shrinkage of the band gap in GaAs/GaAlAs quantum-well material. For both cases it is shown that the inhomogeneous spatial distribution of the nonlinear absorption profile along the direction of propagation of the electric field undergoes a first-order-like phase transition commensurate with the transition of the output intensity from one value to another for fixed input intensity. Stability conditions are presented for the steady states of the output intensity as a function of the input intensity for the cases treated. There is a multiplicity of bistability curves, and the stability analysis produced the expected branches of stable solutions.

20 DISTRIBUTION/AVAILABILITY OF ABSTRACT UNCLASSIFIED/UNLIMITED [X] SAME AS RPT [] DTIC USERS

21 ABSTRACT SECURITY CLASSIFICATION UNCL

22a NAME OF RESPONSIBLE INDIVIDUAL Dr. Charles M. Bowden

22b TELEPHONE (Include Area Code) (205) 876-2650

22c OFFICE SYMBOL AMSMI-RD-RE-OP

Longitudinal spatial inhomogeneities in intrinsic optical bistability due to induced absorption

Charles M. Bowden

Research Directorate, AMSMI-RD-RE-OP, Research, Development, and Engineering Center, U.S. Army
Missile Command, Redstone Arsenal, Alabama 35898-5248

C. C. Sung

Department of Physics, University of Alabama at Huntsville, Huntsville, Alabama 35899

J. W. Haus

Department of Physics, Rensselaer Polytechnic Institute, Troy, New York 12181

J. M. Cook

Department of Physics, Middle Tennessee State University, Murfreesboro, Tennessee 37132

Received June 25, 1987; accepted September 17, 1987

Longitudinal spatial effects in the nonlinear medium are analyzed in a model for mirrorless optical bistability due to induced absorption that treats heat conduction, electromagnetic field propagation, and temperature-dependent absorption. We consider two specific cases: the temperature-induced shift of the absorption peak of bound I_2 excitons in CdS single crystals and the temperature-induced shrinkage of the band gap in GaAs/GaAlAs quantum-well material. For both cases it is shown that the inhomogeneous spatial distribution of the nonlinear absorption profile along the direction of propagation of the electric field undergoes a first-order-like phase transition commensurate with the transition of the output intensity from one value to another for fixed input intensity. Stability conditions are presented for the steady states of the output intensity as a function of the input intensity for the cases treated. There is a multiplicity of bistability curves, and the stability analysis produced the expected branches of stable solutions.

1. INTRODUCTION

There has been a recent surge of interest in intrinsic optical bistability¹ (IOB), i.e., optical bistability that does not depend on external feedback such as from the mirrors of a high- Q cavity. Since the first predictions for the conditions for IOB,^{2,3} other theoretical calculations have expanded on the phenomenon for a wide variety of circumstances.⁴⁻¹⁷ The first reported experimental study of IOB was conducted by Hajto and Janossy¹⁸ in amorphous GeSe₂ due to thermally induced absorption, and this was followed by the experimental observations of Miller *et al.*¹⁹ in GaAs/GaAlAs by tuning just below the band gap. They also analyzed their results in terms of temperature-induced absorption. Bohner *et al.*,²⁰ and almost simultaneously Rossmann *et al.*,²¹ observed IOB in CdS. The presence of IOB in CdS has been interpreted as due primarily to effects of electronic origin owing to saturation of absorption because of the generation of carriers resulting in nonlinear renormalization of the band gap with increasing electromagnetic field intensity.¹⁰ Later, Dagenais and Sharfin observed IOB in CdS at much lower intensities by tuning just below the bound I_2 exciton resonance²² and interpreted their results as due to thermally induced increasing absorption. Since these initial experimental studies were reported, there have been many other reported results of observations of IOB in various materials

with different mechanisms^{23,24} as well as predictions of IOB under other novel conditions. For instance, IOB with atoms densely packed so that dipole-dipole interactions become important has been analyzed by Bowden and co-workers^{11,12,15-17} but not yet experimentally studied.

In this paper we analyze nonlinear longitudinal spatial inhomogeneities associated with IOB due to induced absorption. We treat two specific cases: induced absorption, which results when the incident laser field is tuned just below the bound-exciton resonance of the I_2 bound exciton in thin, uncoated platelets of CdS single crystals, and induced absorption, which results from tuning the laser frequency below the band edge in GaAs/GaAlAs quantum-well structures. For both cases, the plane-wave propagation of the electromagnetic field, coupled with heat conduction and the associated boundary conditions, is used to derive the steady-state longitudinal electric field amplitude, intensity, and temperature and the temperature-dependent absorption distributions in the nonlinear material. It is shown for each case that the longitudinal spatial absorption distribution in the material undergoes a first-order spatial phase transition commensurate with the transition of the system from one bistable output intensity to another for fixed incident intensity. The longitudinal spatial first-order phase transition is generic to IOB and does not exist for optical bistability (OB) in the presence of an optical cavity or an

étalon of high Q . In fact, it rounds out the concept of IOB as an example of a first-order phase transition far from thermodynamic equilibrium. The first analysis of the longitudinal spatial phase transition for a dense two-level atomic system was published by Ben-Aryeh and co-workers.¹⁵⁻¹⁷ With the exception of the recent work by the present authors, all previous treatments have ignored the spatial distribution dependence of the field and temperature in IOB due to induced absorption.

It should be noted here that the predictions of Koch *et al.*²⁵ and subsequent experimental observations of Gibbs *et al.*²⁶ of the stepwise output as a function of pulsed input intensity for CdS, which they describe as "kinks," is not at all the same phenomenon that we describe here. In that case, the sample of CdS (or CdS-doped glass) is excited by a pulse; an instability in the transmission is found to be due to band-gap renormalization. What we discuss for IOB here is a genuine, stationary, first-order spatial phase transition.

In addition to the treatment of the longitudinal spatial phase transition, we discuss the stability conditions of the stationary states for the cases presented. We develop here, for the first time to our knowledge, a linearized stability analysis that takes into account the spatial dependence and intrinsic longitudinal inhomogeneity in IOB.

The model is presented and discussed in Section 2 in terms of coupled constitutive Maxwell and heat-conductivity equations. Section 3 is used to present the results of numerical calculations for IOB in CdS and GaAs/GaAlAs quantum-well material. The linearized stability analysis is developed in Section 4, which takes into account propagation and spatial inhomogeneity. This analysis is applied to the cases treated, and the results are discussed. The final section is used for conclusions and to summarize the results.

2. THE MODEL

Here we review the model presented earlier.^{13,14} Our model for IOB due to induced absorption consists of a set of coupled Maxwell equations for the electric field amplitude inside the nonlinear medium and heat-conductivity equation for the temperature distribution in the material. In the plane-wave limit, the positive-frequency part of the field, E^+ , in the medium is given by

$$E^+(x, t) = [E_F^+(x, t)e^{ikx} + E_B^+(x, t)e^{-ikx}]e^{-i\omega t}, \quad (1)$$

where $E(x, t) = E^+(x, t) + E^-(x, t)$, $(E^+)^* = E^-$, and E_F^+ and E_B^+ are forward- and backward-propagating electric field amplitudes, respectively, and are assumed to be slowly varying functions of x and t . Here $k = k_0\sqrt{\epsilon}$, where k_0 is the wave vector in vacuum and ϵ is the real part of the dielectric function in the medium.

For steady state and in the limit of fast relaxation of the medium, Maxwell's equations in the slowly varying envelope approximation (SVEA) are

$$\frac{1}{c} \frac{\partial E_F^+}{\partial t} + \frac{\partial E_F^+}{\partial x} + \frac{\eta}{2} E_F^+ = 0, \quad (2a)$$

$$-\frac{1}{c} \frac{\partial E_B^+}{\partial t} + \frac{\partial E_B^+}{\partial x} - \frac{\eta}{2} E_B^+ = 0, \quad (2b)$$

where $\eta = \alpha + i\beta$ and α and β are corresponding absorption and dispersion functions in the medium and are related by

the Kramers-Kronig relations. It is to be noted that η is spatially inhomogeneous in the medium and is dependent on the local temperature T . Thus Eqs. (2) are coupled by η . The temperature $T(x)$ is determined by the heat-conduction equation:

$$C_v \frac{\partial T}{\partial t} - \kappa \frac{\partial^2 T}{\partial x^2} = I\alpha, \quad (3)$$

where κ is the heat conductivity, assumed constant and homogeneous, and $I = I(x)$ is the local intensity of the field. In this section and in Section 3 we consider only steady-state solutions, but the time dependence is important in Section 4, where we take up the stability analysis.

Maxwell's equations, Eqs. (2), can be simplified further by using the transformation

$$E_{(F/B)}^+(x) = \bar{E}_{(F/B)}^+(x) \exp\left[\mp \frac{i}{2} \int_0^x dx' \beta(x')\right]. \quad (4)$$

The resulting equations thus have real coefficients, and the dispersion β appears only in the boundary conditions for the field at $x = L$ in terms of a phase factor denoted by

$$\bar{K}L = KL - \frac{1}{2} \int_0^L dx' \beta(x'). \quad (5)$$

Consistent with the SVEA, the intensity I in Eq. (3) can be written in terms of the forward- and backward-propagating fields as

$$I = |E_F^+|^2 + |E_B^+|^2, \quad (6)$$

where the rapidly varying cross term has been neglected.

Equations (2), using the transformation [Eq. (4)], become

$$\frac{\partial \bar{E}_F^+}{\partial x} + \frac{\alpha}{2} \bar{E}_F^+ = 0, \quad (7a)$$

$$\frac{\partial \bar{E}_B^+}{\partial x} - \frac{\alpha}{2} \bar{E}_B^+ = 0, \quad (7b)$$

and (refer to Fig. 1) the associated boundary conditions are

at $x = 0$

$$\bar{E}_F^+(0) + \bar{E}_B^+(0) = E_I^+ + E_R^+, \quad (8a)$$

$$\sqrt{\epsilon}[\bar{E}_F^+(0) - \bar{E}_B^+(0)] = (E_I^+ - E_R^+)\sqrt{\epsilon_0}, \quad (8b)$$

at $x = L$

$$\bar{E}_F^+(L)e^{i\bar{K}L} + \bar{E}_B^+(L)e^{-i\bar{K}L} = E_T^+, \quad (8c)$$

$$\sqrt{\epsilon}[\bar{E}_F^+(L)e^{i\bar{K}L} - \bar{E}_B^+(L)e^{-i\bar{K}L}] = E_T^+\sqrt{\epsilon_0}, \quad (8d)$$

where E_I , E_R , and E_T are the normally incident, reflected, and transmitted field amplitudes, respectively, and ϵ_0 is the dielectric constant of the external medium, whereas ϵ is the linear dielectric constant of the medium.

In terms of the incident intensity I_I and the transmitted intensity I_T , the boundary conditions, Eqs. (8), give

$$I_T = \frac{4 \frac{\epsilon}{\epsilon_0}}{[1 + (\epsilon/\epsilon_0)^{1/2}]^2} I_F(L), \quad (9)$$

$$I_I = \{a^2 I_F(0) + b^2 I_B(0) + 2ab \operatorname{Re}[E_F^+(0)E_B^-(0)]\}, \quad (10)$$

where

$$a = (\epsilon/\epsilon_0)^{1/2} + 1, \quad b = (\epsilon/\epsilon_0)^{1/2} - 1, \quad (11)$$

and

$$I_F(x) = |E_F^+(x)|^2, \quad I_B(x) = |E_B^+(x)|^2, \\ I(x) = |E_F^+(x)|^2 + |E_B^+(x)|^2. \quad (12)$$

For the boundary conditions associated with Eq. (3), we have adopted the following form:

$$H_x[T(x) - T_b] = I(x)\alpha(x) \quad \begin{matrix} x=0 \\ x=L \end{matrix}, \quad (13)$$

where H_0 and H_L are related to the geometry and the thermal resistance at the respective boundaries and T_b is the ambient temperature. Since $\alpha = \alpha[T(x)]$ is a nonlinear function of the temperature in the medium, Eq. (13) constitutes a nonlinear relationship between the temperature T at each boundary and the field intensity I at the respective boundary. Thus the local bistable condition throughout the medium is controlled at the boundaries.

The set of coupled constitutive Maxwell equations and the heat-conductivity equation, Eqs. (2) and (3), together with their associated boundary conditions, Eqs. (8) and (13), represent our model for IOB due to induced absorption. Here we apply this model to two distinct cases, which we treated previously, to discuss a new aspect of the first-order phase transition, namely, the *longitudinal spatial inhomogeneity* associated with the intrinsic local bistability in the medium. The two cases that we shall address are the following: Case A, the situation in which the incident field is tuned, at low field values, just below the absorption resonance for the bound I_2 exciton in CdS single-crystal platelets; and Case B, in which the laser field is tuned just below the band edge in a GaAs/GaAlAs quantum-well structure. With regard to Case A, the change in the nonlinear absorption as a function of the internal field intensity causes nonlinear inhomogeneous heating of the material with a consequent local shift of the absorption peak to lower values with increasing local temperature; whereas in Case B, internal heating of the material causes shrinkage of the band gap to lower values for increasing local temperature.

The model presented here was used previously to analyze both cases. The absorption α and the dispersion β , as functions of local temperature $T(x)$, are, however, of entirely different origin in the two cases and are of completely different functional form. The boundary conditions are also quite different in the two cases. Each case, however, represents a generic prototype, as will become apparent in the development in the next two sections. In Section 3 we discuss results for longitudinal spatial inhomogeneities and first-order phase transitions corresponding to IOB due to induced absorption in the two kinds of system.

3. LONGITUDINAL SPATIAL FIRST-ORDER PHASE TRANSITIONS

A. Case A: CdS

Here we discuss IOB due to induced absorption associated with the resonant absorption nonlinearity in CdS due to the bound I_2 exciton. As previously discussed,¹² we adopt here the empirical form for the function η of Eqs. (2):

$$\eta(x) = \frac{\alpha_0[T(x)]}{1 + i\gamma\{\omega - \omega_0[T(x)]\}}, \quad (14)$$

with the explicit form for the absorption part of Eq. (14) taken from experimental data for $T_b = 7$ K:

$$\alpha = \frac{1}{10} \frac{[3 + 0.04(T - T_b)^2]}{\{1 + [\omega - \omega_0(T)]^2(0.4)^2\}} \quad (15)$$

in units of reciprocal micrometers, where T is in degrees Kelvin and $(\omega - \omega_0)$ is in the unit of reciprocal centimeters. In addition, the following empirical relation is used for the temperature, T , dependence of the peak of the absorption.

$$\omega_0(T) = \omega_0(0) - AT^2. \quad (16)$$

This relation is valid for $0 < T < 40$ K with the parameter values $A = 1/80 \text{ cm}^{-1} \text{ K}^{-2}$ and $\omega_0(0) = 20531 \text{ cm}^{-1}$. The conductivity κ of Eq. (3) is taken as $\kappa = 10^{-4} \text{ W}/\mu\text{m K}$.

As is discussed in Ref. 13, the IOB in this case is extremely sensitive to the heat-conductivity boundary conditions, Eq. (13) and, in fact, is dependent on these conditions, whereas the boundary conditions, Eqs. (8) for the field equations, Eqs. (7), do not cause bistability. We discussed previously that the threshold conditions and hysteresis in the output intensity I_{out} as a function of the input intensity I_{in} can be strongly affected by changing the boundary conditions associated with the heat conduction.

In a manner similar to that discussed in Ref. 13, we have numerically integrated Eqs. (7) and (3), using the associated boundary conditions, Eqs. (8) and (13), and the empirical relations (15) and (16) for $T_b = 0$ and, for Eq. (13), $H_L = H_0/3$. Because the heat-conductivity boundary conditions are suitably chosen at the two ends of the CdS platelet (Fig. 1), we obtain two hysteresis conditions, one due to increasing induced absorption at lower-field values and the other due to decreasing induced absorption at the higher fields. The results are qualitatively the same as those reported earlier and are shown in Fig. 2. The only difference between the results shown in Fig. 2 and those reported earlier¹³ is that in this case we have chosen the ambient temperature $T_b = 0$ for convenience.

The absorption profile $\alpha(x)$ before switching from the high to the low transmission state is shown in curve (a) of Fig. 3, which corresponds to point a in the inset of Fig. 2. After switching to the low transmission state, for the same input-field intensity, the absorption profile $\alpha(x)$ changes to that shown in (b) of Fig. 3, which corresponds to point b of

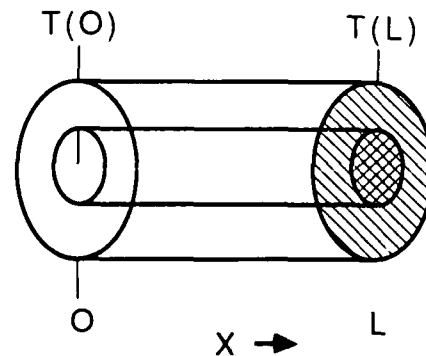


Fig. 1. CdS configuration.

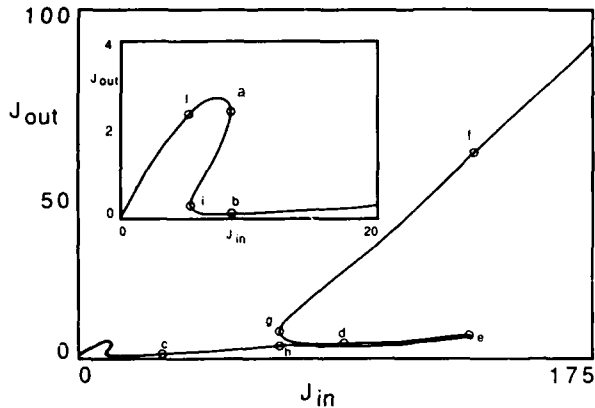


Fig. 2. CdS increasing and decreasing absorption hysteresis in scaled intensities, $J = I/H$: b, lower field (increasing absorption regime); c, higher field (decreasing absorption regime).

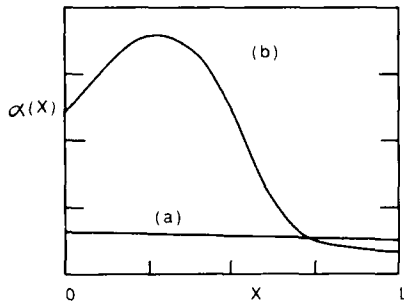


Fig. 3. $\alpha(x)$ for the case of Fig. 2.

Thus the peak of the absorption has swept through the fixed field frequency in the medium for a portion of the nonlinear medium nearest the left-hand boundary, and, consequently, the peak in the spatial distribution of the absorption appears in the medium, just inside the input boundary. The upper and lower curves for $\alpha(x)$ in Fig. 3 are the spatial absorption distribution profiles corresponding to the low and high transmission states for the same value of the threshold input field intensity [Fig. 2 (inset)]. Thus the spatial distribution for the absorption $\alpha(x)$ changes abruptly, corresponding to the switching of the output intensity from high to low transmission, and constitutes a manifestation of the first-order phase transition. This aspect of the phase transition is intrinsic to IOB and, of course, cannot occur in optical bistability that depends on optical feedback, as in a nonlinear Fabry-Perot or ring cavity.

The corresponding intensity distributions in the medium, $I(x)$, are depicted in Fig. 4, and the corresponding slowly varying forward- and backward-propagating field amplitudes are shown in Fig. 5. Also noted is the change in the overall, or average, temperature gradient across the sample by more than a factor of 10 associated with the transition. In the change to the lower transmission state, the temperature in the sample at the input boundary has increased by 13.5 K because of increased absorption, whereas the corresponding temperature at the output boundary has dropped by 3.1 K, which is due to the drastic decrease in field intensity, $I(x)$, near that boundary.

The heat-conductivity boundary condition, Eq. (13), using Eqs. (15) and (16), is shown in Fig. 6 for the input side. This shows that the low-field first-order phase transition

discussed above is primarily associated with the input-side thermal boundary condition, and the qualitative aspect of the behavior depicted in Figs. 2-5 is dependent on this boundary condition. Since there is a boundary condition of the same nature associated with the output boundary, and since, as already noted, the temperature at that boundary has decreased in the transition from the high to low transmission states, it is anticipated that another phase transition will occur at higher input intensity. This transition is shown in Fig. 2 and is due to decreasing absorption.

Thus, as the incident intensity is increased, the peak of the absorption profile, $\alpha(x)$, appears at larger values of x owing to the monotonic increase in the intensity in the medium, $I(x)$, and the distribution $\alpha(x)$ is reshaped longitudinally. The behavior for $\alpha(x)$ is displayed in Fig. 7 for two different input-field values as indicated in Fig. 2 along the lower output-field branch. In other words, as the internal intensity $I(x)$ is increased further throughout the medium, the local absorption peak, $\omega_0[T(x)]$, shifts to lower values, and since the laser frequency ω_L was set at a value less than ω_0 at low input fields, the absorption resonance is swept through the laser frequency for a larger portion of the material medium. This behavior is evident from Eqs. (15) and (16).

The local IOB of the material is expressed explicitly in terms of the boundary condition (Fig. 6). However, because of the large and dominant diffusion in this case, because the heat conductivity κ is large [Eq. (3)], the spatial phase transition corresponds to a kind of Maxwell construction far from thermodynamic equilibrium. Thus the intensity distribu-

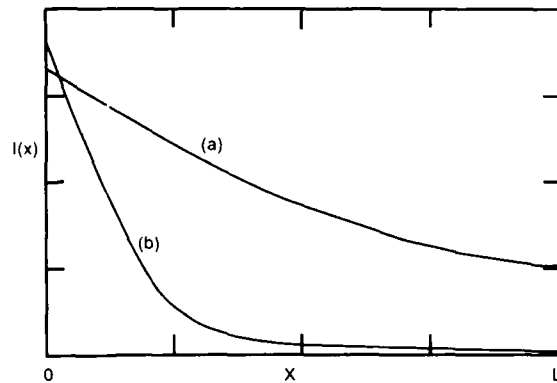


Fig. 4. $I(x)$ for conditions corresponding to Fig. 3: (a) before switching; (b) after switching.

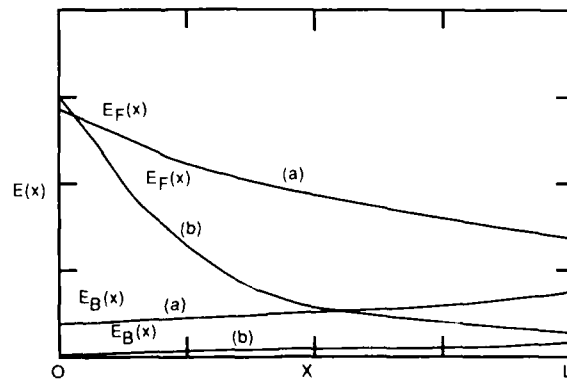


Fig. 5. (a) $E_B(x)$ and $E_F(x)$ before switching (Fig. 3). (b) $E_B(x)$ and $E_F(x)$ after switching (Fig. 3).

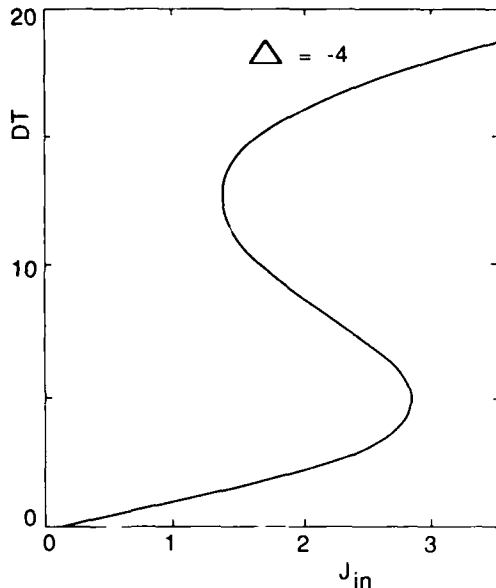


Fig. 6. ΔT versus J_{in} at the input face from Eq. (13) for conditions of Fig. 3. Here, $J_{in} = I/H$.

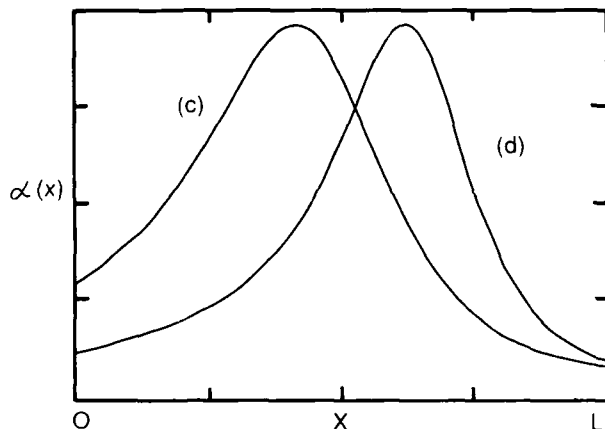


Fig. 7. Input field I_{in} dependence of the nonlinear absorption, $\alpha(x)$.

tion [$I(x)$, Fig. 4] is monotonic. For vanishingly small diffusion in a transport equation, we would expect an abrupt change in $I(x)$, at some $0 < x < L$, introducing a spatial discontinuity in the nonlinear index Δn and a sharp boundary in the material between two spatially separated phases. This kind of phase transition was referred to earlier.¹⁷ The case treated here is for the opposite limit, i.e., large diffusion, which is the natural situation for thermally induced absorption.

A second, or high-field, threshold is reached, which is shown in Fig. 2 for the output intensity I_{out} versus the input intensity I_{in} . The spatial absorption profiles at threshold, corresponding to the low and high transmission states for the same threshold input field, are shown in Fig. 8. In this case, the absorption peak is switched out of the medium as the input field is increased, and, in contrast to the low-field phase transition, this situation corresponds to switching due to decreasing absorption. Thus the hysteresis loop is counterclockwise, as opposed to the clockwise hysteresis associated with the low-input-field transition, which is due to increasing absorption.

It is noted that the temperature at the output boundary has increased by nearly a factor of 4, where, in contrast, the temperature at the input boundary remains nearly fixed with respect to the transition. Thus the transition discussed here is associated primarily with the output boundary condition, Eq. (13). The large increase in the temperature at the output boundary is due to the relatively large increase in the intensity $I(x)$ near the output boundary. Here, the absolute value for the average temperature gradient across the sample drops in the transition from the low to the high transmission state. Noted here is an actual inversion of the gradient, so the temperature at the output is greater than the temperature at the input, i.e., $T(L) > T(0)$.

If the input field is decreased from a high value, an intermediate field threshold is reached, as depicted in Fig. 2. Figure 9 shows the absorption profile $\alpha(x)$ for the high and low transmission states, respectively, at the indicated threshold input field. Here the peak of the absorption profile $\alpha(x)$ switches back into the material in the transition from the high to the low transmission state (Fig. 9). It is interesting to compare the profile, $\alpha(x)$, in the low transmission states in Figs. 9 and 8. In the former case, the absorption peak is located deeper into the material as compared with the latter case, which is, of course, expected, owing to the difference in the respective input fields.

We note, in connection with Fig. 9, that $T(0)$ remains approximately fixed but $T(L)$ decreases markedly through the transition, indicating that the phase transition associated with the high-field, counterclockwise hysteresis is associ-

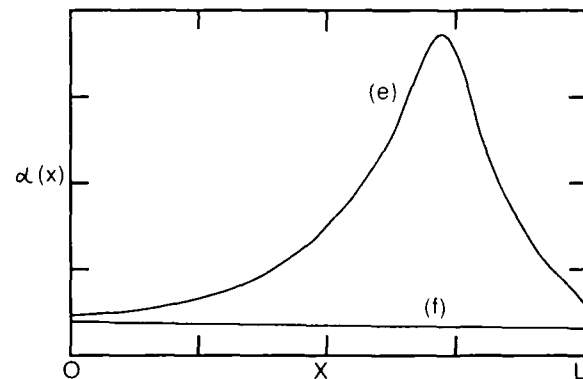


Fig. 8. $\alpha(x)$ at higher input field, second threshold: (e) low transmission (Fig. 2); (f) high transmission (Fig. 2).

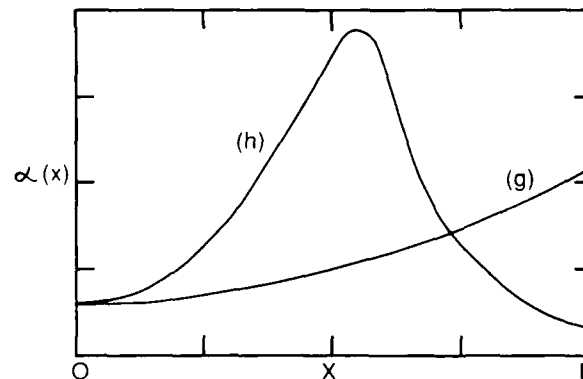


Fig. 9. $\alpha(x)$ at lower input-field threshold in high-input-field regime: (g) high transmission (Fig. 2); (h) low transmission (Fig. 2).

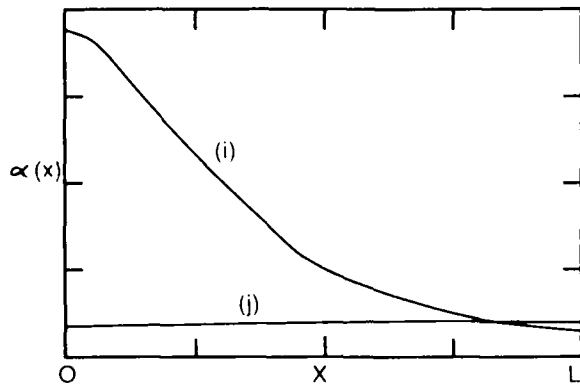


Fig. 10. $\alpha(x)$ at lowest input-field threshold: (i) low transmission (Fig. 2); (ii) high transmission (Fig. 2).

ated primarily with the output-side heat-conductivity boundary conditions.

Finally, for still lower values of the input-field intensity, the lowest field threshold is reached, as shown in Fig. 2. Figure 10 shows the absorption profiles $\alpha(x)$ in the low and high transmission states, respectively. Here, the temperature $T(L)$ changes relatively little, indicating that the transition is controlled primarily by the heat-conductivity boundary conditions at the input boundary.

B. Case B: GaAs/GaAlAs

For Case B we discuss IOB due to induced absorption using the nonlinear absorption associated with tuning in the region of the band gap in GaAs/GaAlAs multiple-quantum-well structures. Here we use the empirically determined absorption function

$$\alpha(\omega, T) = \alpha_l \exp\left[\frac{-(\omega - \Omega_l)^2}{2\Gamma_l}\right] + \alpha_h \exp\left[\frac{-(\omega - \Omega_h)^2}{2\Gamma_h}\right] + 2\alpha_c \left[1 + \exp\left(\frac{\Omega_c - \omega}{k_c}\right)\right]^{-1} \times [1 + \exp(-2\pi R_y^{1/2} |\Omega_c - \omega|^{-1/2})]^{-1}, \quad (17)$$

where all the constants, $\alpha_l, \Gamma_l, \alpha_h, \Gamma_h, \Omega_l, \Omega_h, \Omega_c, \alpha_c, \Gamma_c,$ and $R_y,$ are given in Ref. 14. The band gap has the temperature, $T,$ dependence,

$$\Omega_c(T) = \Omega_c(0) - \frac{AT^2}{T+B}, \quad (18)$$

where $\Omega_c(0) = 1.51216$ eV, $A = 8.87 \times 10^{-4}$ K⁻¹, $B = 572$ K, and T is in units of K. The results discussed here pertain exactly and explicitly to the calculations and results reported earlier and appear in Ref. 14. Equation (17), $\alpha(T)$ versus $T,$ is shown in Fig. 11.

The geometry of the configuration is discussed in Ref. 14. Equations (2) and (3) are integrated across the sample under steady-state conditions and with the appropriate boundary conditions, as discussed in Ref. 14. The heat-conductivity boundary conditions, Eq. (13), are shown for this case in Figs. 12(a) and 12(b) for the input boundary and the output boundary of the sample, respectively. The corresponding output intensity I_{out} versus the input intensity I_{in} is represented in Fig. 13. These results are identical to the results reported earlier but are reproduced here for clarity.

The absorption profile, $\alpha(x),$ is shown in Fig. 14 for six of the eight threshold conditions depicted in Figs. 12 and 13. At the low-input-field threshold, the transition from the high to the low transmission state, denoted by a and b, respectively, in Figs. 12 and 13, corresponds to the change in the absorption distribution, $\alpha(x),$ in the material denoted by curves a and b in Fig. 14. Thus the absorption profile of the band edge switches into the medium as the sample switches from the high to the low transmission state. The corresponding transition at the input boundary is noted in Fig. 12, and it is seen that the transition is associated primarily with

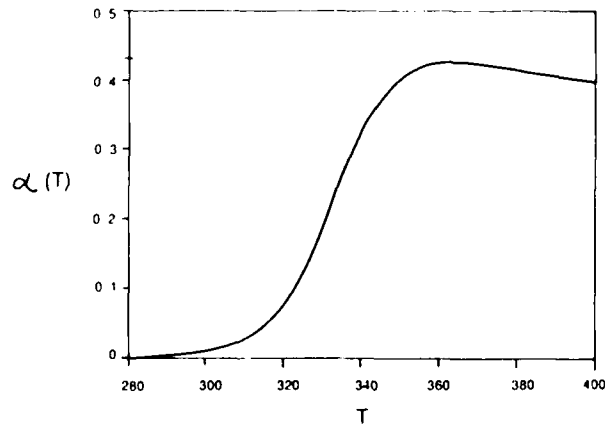


Fig. 11. $\alpha(T)$ versus T for GaAs/GaAlAs.

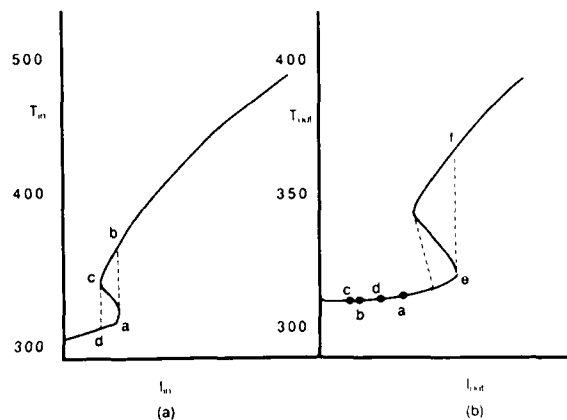


Fig. 12. (a) T_{in} versus I_{in} for GaAs/GaAlAs. (b) T_{out} versus I_{out} for GaAs/GaAlAs.

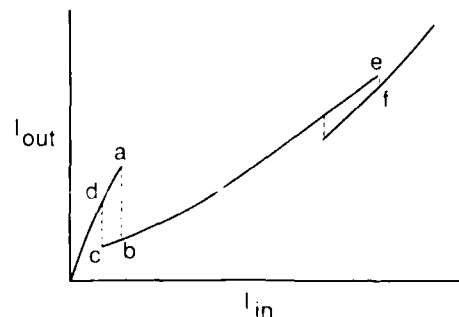


Fig. 13. I_{out} versus I_{in} for conditions of Figs. 11 and 12.

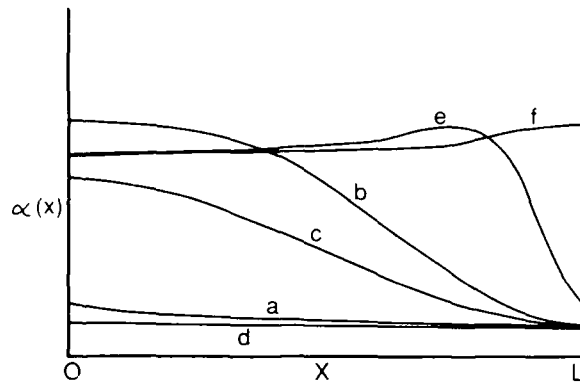


Fig. 14. $\alpha(x)$ for GaAs/GaAlAs. The conditions are the same as for Figs. 11-13.

the input boundary, whereas the corresponding changes at the output boundary are relatively minor.

For higher values of the incident field intensity, the edge of the absorption profile penetrates deeper into the medium until the higher field threshold is reached, denoted by e-f of Figs. 12 and 13. The corresponding absorption profiles $\alpha(x)$ for the high- and low-transmission states for this threshold condition are shown in Fig. 14 and are denoted by e and f, respectively. Thus the edge of the absorption profile $\alpha(x)$ is swept out of the medium. This transition is controlled primarily by the boundary conditions at the output boundary, as noted in Fig. 12.

Unlike the situation for Case A, for which $\alpha(x)$ has a well-defined absorption maximum, the high- and low-field transitions each correspond to transitions due to increasing absorption and thus give rise to clockwise hysteresis loops. In other words, as the incident field intensity is increased, the absorption distribution $\alpha(x)$ in the material increases monotonically to saturation.

In this section we have treated the longitudinal spatial first-order phase transition associated with the spatial dependence of the absorption distribution $\alpha(x)$ in the material for IOB due to induced absorption. This gives rise to a kind of Maxwell construction in the material far from thermodynamic equilibrium and rounds out the profile of a first-order phase transition interpretation of IOB. This bears out the intrinsic nature of the phase transition in IOB.

In Section 4 we discuss the stability conditions for the cases treated in this section.

4. STABILITY ANALYSIS

We shall address the stability analysis to the CdS system; the identical procedure is applicable to the GaAs/GaAlAs system treated here, and the results are qualitatively the same. Considering the general solution of the physical quantities such as $E_{F,B}(x, t)$ as the sum of the steady-state solution $[E_{F,B}(x)]_s$ obtained earlier and a small transient variation, $\delta E_{F,B}(x, t)$, i.e.,

$$E_{F,B}(x, t) = [E_{F,B}(x)]_s + \delta E_{F,B}(x, t),$$

$$T(x, t) = [T(x, t)]_s + \delta T(x, t),$$

we obtain from Eqs. (2)

$$\frac{1}{c} \frac{\partial}{\partial t} \delta E_{F,B}(x, t) \pm \frac{\partial}{\partial x} \delta E_{F,B}(x, t) + \frac{n}{2} \left|_s \delta E_{F,B}(x, t) + \frac{1}{2} \left(E_{F,B} \frac{\partial n}{\partial T} \right) \delta T = 0 \quad (19)$$

and

$$C_v \frac{\partial \delta T}{\partial t} - k \frac{\partial^2}{\partial x^2} \delta T = I \frac{\partial \alpha}{\partial T} \left|_s \delta T + 2\alpha(E_F) \delta E_F + 2\alpha(E_B) \delta E_B, \quad (20)$$

where $()_s$ denotes the steady state and we have dropped the superscript + for convenience. The usual stability analysis is carried out by solving the linearized differential equations and determining a set of eigenvalues $\{\lambda\}$ that express the time development through the relations

$$\delta E_{F,B}(x, t) = \delta \tilde{E}_{F,B}(x) e^{\lambda t}, \quad \delta T(x, t) = \delta \tilde{T}(x) e^{\lambda t}. \quad (21)$$

The numerical solution corresponding to this procedure has been carried out by one of the authors²⁷ using finite-difference methods. We present here a different approach based on approximations intrinsic to the particular systems treated here. This approach, though less general than the conventional one, has the advantage of producing transparent analytical results. The numerical results²⁷ are in agreement with those given here.

Because of the high diffusion limit applied to the cases treated here, the heat-conduction equation, Eq. (3), cannot contribute to instabilities associated with the steady state. This is evidenced by the fact that the temperature gradient in the material is essentially linear. Furthermore, as we have demonstrated in the previous sections, the bistable behavior of the system is entirely associated with the multi-valued solutions of the boundary values at the two ends of the sample [Eq. (13)]. Consequently, under the approximation that bistable switching is independently controlled by the nonlinear boundary conditions at the two end faces of the material, we analyze the stability at $x = 0$ and at $x = L$ separately.

First, consider Eq. (19) evaluated at $x = 0$:

$$\frac{\lambda}{c} \delta \tilde{E}_{F,B}(x) \pm \frac{\partial}{\partial x} \delta \tilde{E}_{F,B}(x) + \frac{n}{2} \left|_s \delta \tilde{E}_{F,B}(x) + \frac{1}{2} \left(E_{F,B} \frac{\partial n}{\partial T} \right) \delta \tilde{T}(x) = 0; \quad (22)$$

and $\delta \tilde{T}(0)$ and $\delta \tilde{E}_{F,B}(x)$ at $x = 0$ are related through Eqs. (8) and (13):

$$\delta \tilde{T}(x) = \alpha \left[1 - \frac{\partial \alpha}{\partial T} I(x) \right]^{-1} \left|_s [E_B(x) + R E_F(x)] \delta \tilde{E}_B(x), \quad (23a)$$

$$\delta \tilde{E}_B(x) = \frac{1}{R} \delta E_F(x), \quad (23b)$$

where the intensity I is normalized by taking the surface conductivity to be unity and $R = (\sqrt{\epsilon} - 1)/(\sqrt{\epsilon} + 1)$.

If we express $\delta \tilde{E}_{F,B}(x)$ in terms of their Fourier transforms,

$$\delta \tilde{E}_{F,B}(x) = \sum_{n=0} \exp(\pm 2\pi i n x / L) \delta \tilde{E}_{F,B}^{(n)}, \quad (24)$$

where the upper (lower) sign is taken for $\delta\tilde{E}_F$ ($\delta\tilde{E}_B$), and eliminate $\delta\tilde{T}(x)$, using Eq. (23a), in Eqs. (22), these equations yield

$$(\lambda + ik_n c + g_F)\delta\tilde{E}_F^{(n)} = 0, \quad (25a)$$

$$(\lambda - ik_n c + g_B)\delta\tilde{E}_B^{(n)} = 0, \quad (25b)$$

where, at $x = 0$,

$$g_F = \alpha(0) \frac{\left[1 + 2 \left(\frac{\partial \alpha}{\partial T} \right)_{x=0} \frac{E_B(0)E_{in}/(\sqrt{\epsilon} - 1)}{\alpha(0)} \right]}{\left\{ 1 - \left(\frac{\partial \alpha}{\partial T} \right)_{x=0} \frac{[T(0) - T_B]}{\alpha(0)} \right\}}, \quad (26a)$$

$$g_B = \alpha(0) \frac{\left[1 - 2 \left(\frac{\partial \alpha}{\partial T} \right)_{x=0} \frac{E_F(0)E_{in}/(\sqrt{\epsilon} - 1)}{\alpha(0)} \right]}{\left\{ 1 - \left(\frac{\partial \alpha}{\partial T} \right)_{x=0} \frac{[T(0) - T_B]}{\alpha(0)} \right\}}. \quad (26b)$$

Notice that if Eq. (24) and a similar expansion for $\delta\tilde{T}(x)$ are used in Eqs. (19) and (20), the conventional approach to instabilities emerges, whereas replacing the physical quantities $n|_s$, $\alpha|_s$, $E_B|_s$, etc. by average values in the medium leads to results in the mean-field approximation.

As is evident from Eqs. (25) and (26), stability of the phase transition associated with the left-hand boundary, i.e., $x = 0$, is determined by the sign of g_F and g_B , i.e., both g_F and g_B must be positive to warrant a stable solution. An analysis of g_F and g_B shows that the dominant factor in the determination of the sign is

$$A_0 \equiv 1 - (\partial\alpha/\partial T)_{x=0} [T(0) - T_B]/\alpha(0). \quad (27)$$

The reason for this is that the numerator of g_F is close to one, since $E_B(0)$ is small, whereas the numerator of g_B is always slightly greater than the denominator. Thus the stable solutions are given by

$$A_0 > 0 \quad \text{at} \quad x = 0. \quad (28)$$

It is noted that $A_0 = 0$ is the exact location of the turning point (Fig. 6) at $x = 0$. Similar results pertain to the right-hand boundary, i.e., at $x = L$, and the phase transition associated with that boundary.

The stable solutions are defined as the region where both $\text{Im}(\lambda_n)$ are negative. Then the unstable region in our problem is simply the middle branch in the OB curve, as expected.

5. CONCLUSIONS

We have demonstrated and discussed the existence of a spatial longitudinal first-order phase transition generic to IOB due to induced absorption and the associated heat-conductivity boundary conditions. The phenomenon is indeed intrinsic to IOB and is nonexistent in the good-cavity limit.

Here, we have addressed the case of the high-diffusion limit characterized by a large Maxwell construction region in the longitudinal spatial variable characteristic of IOB due to induced absorption. This is contrasted with the low-diffusion limit treated earlier,¹⁷ which exhibits an abrupt change in the longitudinal spatial dependence of the material variables at the phase transition. This behavior rounds out the picture of an intrinsic first-order phase transition in a sys-

tem consisting of the radiation field interacting with matter far from thermodynamic equilibrium.

The spatial first-order phase transition may be observed directly by low-intensity transverse field absorption in the material. We anticipate that experiments will be conducted in the future to test these fundamental interpretations.

REFERENCES

1. C. M. Bowden, "Intrinsic optical bistability," in *Quantum Optics IV*, J. D. Harvey and D. F. Walls, eds., Vol. 12 of Springer Proceedings in Physics (Springer-Verlag, New York, 1986), pp. 139-150; "Recent developments in optical bistability," in *Optical Chaos*, J. Chrostowski and N. B. Abraham, eds., Proc. Soc. Photo-Opt. Instrum. Eng. **667**, 56 (1976).
2. C. M. Bowden and C. C. Sung, "First and second order phase transitions in the Dicke model: relation to optical bistability," *Phys. Rev. A* **19**, 2392 (1979).
3. C. M. Bowden, "Optical bistability based upon atomic correlations in a small volume," in *Optical Bistability*, C. M. Bowden, M. Cifan, and H. R. Robl, eds. (Plenum, New York, 1981), pp. 405-429.
4. C. Flytzanis and C. S. Tang, "Light-induced critical behavior in the four-wave interaction in nonlinear systems," *Phys. Rev. Lett.* **45**, 441 (1980).
5. J. A. Goldstone and E. Garmire, "Intrinsic optical bistability in nonlinear media," *Phys. Rev. Lett.* **53**, 910 (1984).
6. B. Ritchie and C. M. Bowden, "Dynamical response and switching of an optically bistable anharmonic oscillator," *Phys. Rev. A* **32**, 2293 (1985).
7. J.-M. Yuan, E. Liu, and M. Tung, "Bistability and hysteresis in laser-driven polyatomic molecules," *J. Chem. Phys.* **79**, 5034 (1983).
8. E. Liu and J.-M. Yuan, "Chaotic attractor with hysteresis in laser-driven molecules," *Phys. Rev. A* **29**, 2257 (1984).
9. F. Henneberger and H. Rossmann, "Resonatorless optical bistability based on increasing nonlinear absorption," *Phys. Status Solidi B* **121**, 685 (1984).
10. H. E. Schmidt, H. Haug, and S. W. Koch, "Theoretical explanation of the absorptive optical bistability in semiconductors due to bandgap shrinkage," *Appl. Phys. Lett.* **44**, 787 (1984).
11. F. A. Hopf, C. M. Bowden, and W. H. Louisell, "Mirrorless optical bistability with the use of the local-field correction," *Phys. Rev. A* **29**, 2591-2596 (1985).
12. F. A. Hopf and C. M. Bowden, "Heuristic stochastic model of mirrorless optical bistability," *Phys. Rev. A* **32**, 268 (1985).
13. J. W. Haus, C. C. Sung, C. M. Bowden, and J. M. Cook, "Model for mirrorless optical multiple bistability due to increasing and decreasing absorption," *J. Opt. Soc. Am. B* **2**, 1920 (1985).
14. Y. Q. Li, C. C. Sung, J. W. Haus, and C. M. Bowden, "Model for mirrorless optical bistability in multiple-quantum-well GaAs/GaAlAs due to induced absorption," *J. Opt. Soc. Am. B* **3**, 1206 (1986).
15. Y. Ben-Aryeh and C. M. Bowden, "Mirrorless optical bistability in a spatially distributed collection of two-level systems," *Opt. Commun.* **59**, 224 (1986).
16. Y. Ben-Aryeh, C. M. Bowden, and J. C. Englund, "Intrinsic optical bistability in collections of spatially distributed two-level atoms," *Phys. Rev. A* **34**, 3917 (1986).
17. Y. Ben-Aryeh, C. M. Bowden, and J. C. Englund, "Longitudinal spatial first-order phase transition in a spatially distributed two-level system interacting with a coherent field," *Opt. Commun.* **61**, 147 (1987).
18. J. Hajto and I. Janossy, "Optical bistability observed in amorphous semiconductor films," *Phil. Mag.* **B 47**, 347 (1983).
19. D. A. B. Miller, A. C. Gossard, and W. Wiegmann, "Optical bistability due to increasing absorption," *Opt. Lett.* **9**, 162 (1984).
20. K. Bohnert, H. Kalt, and C. Klingshirm, "Intrinsic absorptive optical bistability in CdS," *Appl. Phys.* **43**, 1088 (1983).
21. H. Rossmann, F. Henneberger, and H. Voigt, "Memory effect in the excitonic transmission of CdS," *Phys. Status Solidi B* **115**, k63 (1983).

- 22. M. Dagenais and W. F. Sharfin, "Cavityless optical bistability due to light-induced absorption in cadmium sulfide," *Appl. Phys. Lett.* **45**, 210 (1984).
- 23. H. M. Gibbs, *Optical Bistability: Controlling Light with Light* (Academic, New York, 1985).
- 24. H. M. Gibbs, P. Mandel, N. Peyghambarian, and S. D. Smith, eds., *Optical Bistability III*, Vol. 8 of *Springer Proceedings in Physics* (Springer-Verlag, New York, 1986).
- 25. S. W. Koch, H. E. Schmidt, and H. Haug, "Optical bistability due to induced absorption: propagation dynamics of excitation profiles," *Appl. Phys. Lett.* **45**, 932 (1984).
- 26. H. M. Gibbs, G. R. Olbright, N. Peyghambarian, H. E. Schmidt, S. W. Koch, and H. Haug, "Kinks: longitudinal excitation discontinuities and increasing absorption optical bistability," *Phys. Rev. A* **32**, 692 (1985).
- 27. J. W. Haus and T. K. Tran, "Computational method for intrinsic bistability. Steady-state solutions in their stability," submitted to *Comput. Phys.*

Accession For	
NTIS GRA&I	<input checked="" type="checkbox"/>
DTIC TAB	<input type="checkbox"/>
Unannounced	<input type="checkbox"/>
Justification	
By	
Distribution/	
Availability Codes	
Dist	Avail and/or Special
A-1 20	

